

Energy dependent chemical potentials of light particles and quarks from yield ratios of antiparticles to particles in high energy collisions

Hai-Ling Lao¹, Ya-Qin Gao², Fu-Hu Liu^{1,*}

¹*Institute of Theoretical Physics & State Key Laboratory of Quantum Optics and Quantum Optics Devices, Shanxi University, Taiyuan, Shanxi 030006, China*

²*Department of Physics, Taiyuan University of Science and Technology, Taiyuan, Shanxi 030024, China*

Abstract: We collect the yields of charged pions (π^- and π^+), charged kaons (K^- and K^+), anti-protons (\bar{p}), and protons (p) produced in mid-rapidity interval (in most cases) in central gold-gold (Au-Au), central lead-lead (Pb-Pb), and inelastic or non-single-diffractive proton-proton (pp) collisions at different collision energies. The chemical potentials of light particles and quarks are extracted from the yield ratios, π^-/π^+ , K^-/K^+ , and \bar{p}/p , of antiparticles to particles over an energy range from a few GeV to above 10 TeV. At a few GeV (~ 4 GeV), the chemical potentials show, and the yield ratios do not show, different trends comparing with those at other energies, though the limiting values of the chemical potentials and the yield ratios at very high energy are 0 and 1 respectively.

Keywords: chemical potentials of light particles; chemical potentials of light quarks; yield ratios of antiparticles to particles

PACS 14.40.Aq, 14.65.Bt, 25.75.-q

1 Introduction

Chemical potential (μ_{baryon}) of baryon in high energy collisions is a very interesting and important topic studied by researchers in the fields of particle and nuclear physics. Combining with temperature (T_{ch}) at chemical freeze-out, one can study the quantum chromodynamics (QCD) phase diagram in the plane of T_{ch} against μ_{baryon} for the phase transition from hadronic matter to quark-gluon plasma (QGP) [1–4]. It is expected that this phase transition possibly happens over a center-of-mass energy per nucleon pair, $\sqrt{s_{NN}}$, range from a few GeV to dozens of GeV. The purpose of the beam energy scan (BES) performed at the Super Proton Synchrotron (SPS) and the Relativistic Heavy Ion Collider (RHIC) is to search for the critical energy at which the phase transition from hadronic matter to QGP had happened in all probability [5–8]. The BES energies at the SPS reach or close to the Alternating Gradient Synchrotron (AGS) energy.

Combining with the AGS, SPS (at its BES), and RHIC (at its BES), one can study the QCD phase diagram over an energy range from a few GeV to 200 GeV [1–4]. In particular, the Large Hadron Collider (LHC) has extended the energy range to a few TeV and even above 10 TeV [9–12]. It is convenient for researchers to

study the QCD phase transition further. At the same time, the excitation functions of T_{ch} and μ_{baryon} (the energy dependent T_{ch} and μ_{baryon}) can be studied in the mentioned energy range. Generally, the values of T_{ch} and μ_{baryon} in given collisions can be obtained from the yield ratios of antiparticles to particles in a given rapidity interval and transverse momentum range. Although the chemical potentials of other particles such as mesons can also be obtained from the yield ratios of antiparticles to particles, few chemical potentials of mesons have been studied in literature. This enlightens the present work.

We are interested in the chemical potentials of different types of particles in high energy collisions, which can be obtained from the yield ratios of antiparticles to particles in a particular form. We are also interested in the chemical potentials of different flavors of quarks, which can also be obtained from the same yield ratios of antiparticles to particles. It is expected that chemical potentials of particles (or quarks) change with the increase of collision energy. The excitation function (the dependence on collision energy) of chemical potentials are particularly interesting and worthy of study. From the chemical potentials of particles (or quarks), we can evaluate the relative densities of final particles (or produced quarks) at different energies. These relative

*E-mail: fuhuliu@163.com; fuhuliu@sxu.edu.cn

densities are useful in the understanding of interacting mechanism. Because of the data of yield ratios being very limited, we can only obtain the chemical potentials of some particles and quarks conveniently.

In this paper, we collect the yields of charged pions (π^- and π^+), charged kaons (K^- and K^+), anti-protons (\bar{p}), and protons (p) produced in mid-rapidity interval (in most cases) in central gold-gold (Au-Au) [3, 13–23], central lead-lead (Pb-Pb) [24–29], and inelastic (INEL) or non-single-diffractive (NSD) proton-proton (pp) collisions [3, 30–34] over a center-of-mass energy per nucleon pair, $\sqrt{s_{NN}}$, range from a few GeV to above 10 TeV. The chemical potentials of light particles and quarks are extracted from the yield ratios, π^-/π^+ , K^-/K^+ , and \bar{p}/p , of antiparticles to particles, where the symbol of a given particle is used for its yield for the purpose of simplicity. The energy dependent chemical potentials of light particles and quarks are obtained due to the yield ratios.

2 The method and formalism

To extract the chemical potentials of light particles and quarks, we need to know the yield ratios of antiparticles to particles. Although we can obtain the yield ratios from the normalization constants of transverse momentum spectra for different particles, the quantity of work is huge if we analyze the spectra over a wide energy range. A direct and convenient method is to collect the values of yield ratios from the experiments performed at the AGS, SPS at its BES, RHIC at its BES, and LHC by productive international collaborations, though some yield ratios are not available.

Because of the same formula on the relation between the yield ratio and chemical potential being used in our previous work [35] and the present work, some repetitions are ineluctable to give a whole representation of the present work. According to the statistical arguments based on the chemical and thermal equilibrium, one has the relation between antiproton to proton yield ratio to be [20, 36, 37]

$$\frac{\bar{p}}{p} = \exp\left(-\frac{2\mu_p}{T_{ch}}\right) \approx \exp\left(-\frac{2\mu_{baryon}}{T_{ch}}\right) \quad (1)$$

which is within the thermal and statistical model [36, 37], where μ_p is the chemical potential of proton and

$$T_{ch} = T_{lim} \frac{1}{1 + \exp[2.60 - \ln(\sqrt{s_{NN}})/0.45]} \quad (2)$$

is empirically obtained in the framework of a statistical

thermal model of non-interacting gas particles with the assumption of Boltzmann-Gibbs statistics [1, 2, 38, 39], where $\sqrt{s_{NN}}$ is in the units of GeV and the “limiting” temperature $T_{lim} = 0.164$ GeV.

We would like to point out that Eq. (1) obtained in the statistical thermal model is due to the Boltzmann approximation and the relation to isospin effect. Eq. (2) is due to the Boltzmann approximation in the employ of grand-canonical ensemble, though the employs of canonical ensemble and mix-strangeness canonical ensemble being also considerable. As descriptions on chemical freeze-out, Eqs. (1) and (2) do not include particles with high transverse momenta ($>2-3$ GeV/ c) which are produced in hard scattering process at initial stage and leave the interacting system before chemical freeze-out. The particles taken part in chemical freeze-out should have low transverse momenta ($<2-3$ GeV/ c) and obey the Boltzmann-Gibbs statistics.

According to Eq. (1), the yield ratios of antiparticles to particles for other hadrons with together (anti)protons can be written as

$$k_j \equiv \frac{j^-}{j^+} = \exp\left(-\frac{2\mu_j}{T_{ch}}\right), \quad (3)$$

where k_j denotes the yield ratio of antiparticles to particles of the kind j , and $j = \pi, K, p, D$, and B listed orderly due to their masses. The symbol μ_j represents the chemical potential of particle j . To obtain chemical potentials of quarks, the above five hadrons and their antiparticles are enough. Because of the lifetimes of particles contained top quark being very short to measure, we shall not discuss the top quark related particles, top quark itself, and their chemical potentials.

Let μ_q denote the chemical potential for quark flavor, where $q = u, d, s, c$, and b represent the up, down, strange, charm, and bottom quarks, respectively. The values of μ_q are then expected from these relations. According to refs. [40, 41], based on the same chemical freeze-out temperature, the yield ratios in terms of

quark chemical potentials are

$$\begin{aligned}
k_\pi &= \exp\left[-\frac{(\mu_u - \mu_d)}{T_{ch}}\right] / \exp\left[\frac{(\mu_u - \mu_d)}{T_{ch}}\right] \\
&= \exp\left[-\frac{2(\mu_u - \mu_d)}{T_{ch}}\right], \\
k_K &= \exp\left[-\frac{(\mu_u - \mu_s)}{T_{ch}}\right] / \exp\left[\frac{(\mu_u - \mu_s)}{T_{ch}}\right] \\
&= \exp\left[-\frac{2(\mu_u - \mu_s)}{T_{ch}}\right], \\
k_p &= \exp\left[-\frac{(2\mu_u + \mu_d)}{T_{ch}}\right] / \exp\left[\frac{(2\mu_u + \mu_d)}{T_{ch}}\right] \\
&= \exp\left[-\frac{2(2\mu_u + \mu_d)}{T_{ch}}\right], \\
k_D &= \exp\left[-\frac{(\mu_c - \mu_d)}{T_{ch}}\right] / \exp\left[\frac{(\mu_c - \mu_d)}{T_{ch}}\right] \\
&= \exp\left[-\frac{2(\mu_c - \mu_d)}{T_{ch}}\right], \\
k_B &= \exp\left[-\frac{(\mu_u - \mu_b)}{T_{ch}}\right] / \exp\left[\frac{(\mu_u - \mu_b)}{T_{ch}}\right] \\
&= \exp\left[-\frac{2(\mu_u - \mu_b)}{T_{ch}}\right]. \tag{4}
\end{aligned}$$

According to Eqs. (3) and (4), the chemical potentials of particles and quarks can be obtained, respectively, in terms of yield ratios of antiparticles to particles. The chemical potential of particle j is simply given by

$$\mu_j = -\frac{1}{2}T_{ch} \cdot \ln(k_j). \tag{5}$$

The chemical potentials of quarks q are complicatedly a little. We have

$$\begin{aligned}
\mu_u &= -\frac{1}{6}T_{ch} \cdot \ln(k_\pi \cdot k_p), \\
\mu_d &= -\frac{1}{6}T_{ch} \cdot \ln(k_\pi^{-2} \cdot k_p), \\
\mu_s &= -\frac{1}{6}T_{ch} \cdot \ln(k_\pi \cdot k_K^{-3} \cdot k_p), \\
\mu_c &= -\frac{1}{6}T_{ch} \cdot \ln(k_\pi^{-2} \cdot k_p \cdot k_D^3), \\
\mu_b &= -\frac{1}{6}T_{ch} \cdot \ln(k_\pi \cdot k_p \cdot k_B^{-3}). \tag{6}
\end{aligned}$$

Because of the limited data in extracting chemical potentials of some quarks, only the energy dependent chemical potentials of light particles such as π , K , and p , as well as light quarks such as u , d , and s in an energy range covered the AGS, SPS (at its BES), RHIC (at its BES), and LHC are obtained in the present work. That is to say that, in the present work, only the excitation functions of μ_π , μ_K , μ_p , μ_u , μ_d , and μ_s are studied over

an energy range from a few GeV to above 10 TeV. For central Au-Au (Pb-Pb) collisions and INEL or NSD pp collisions, the energy ranges are not completely corresponding to each other.

It should be noted that other yield ratios such as $\bar{\Lambda}/\Lambda$, $\bar{\Sigma}/\Sigma$, and $\bar{\Omega}/\Omega$ do extract only chemical potentials of light quarks due to the fact that their constituent quarks are only light quarks, which are not needed in the present work in particular. Although these yield ratios are available in experiments at some energies, they will not be analyzed by us.

3 Results and discussion

The yield ratios, π^-/π^+ , K^-/K^+ , and \bar{p}/p , of antiparticles to particles produced in mid-rapidity interval (in most cases) in central Au-Au, central Pb-Pb, and INEL or NSD pp collisions at the AGS, SPS, RHIC, and LHC are shown in Figs. 1(a), 1(b), and 1(c), respectively. The circles, squares, triangles, and stars denote the data measured in Au-Au collisions in mid-rapidity interval from $|y| < 0.05$ to $|y| < 0.4$ and centrality 0–5% by the E895, E866, and E917 Collaborations [13–15] at the AGS, in mid-rapidity interval $|y| < 0.4$ and centrality 0–10% by the E802 and E866 Collaboration [16, 17] at the AGS, in mid-pseudorapidity interval $|\eta| < 0.35$ and centrality 0–5% by the PHENIX Collaboration [18–20], and in mid-rapidity interval from $|y| < 0.1$ to $|y| < 0.5$ and centrality from 0–5% to 0–10% by the STAR Collaborations [3, 21–23] at the RHIC, respectively. The circles, squares, and triangles with acial crosses denote the data measured in Pb-Pb collisions in mid-rapidity interval from $0 < y < 0.2$ or $|y| < 0.1$ to $|y| < 0.6$ and centrality from 0–5% to 0–7.2% by the NA49 Collaboration [24–27] at the SPS, in mid-rapidity interval from $|y| < 0.5$ to $|y| < 0.85$ and centrality 0–3.7% by the NA44 Collaboration [28] at the SPS, and in mid-rapidity interval $|y| < 0.5$ and centrality 0–5% by the ALICE Collaboration [29] at the LHC, respectively. The circles, squares, triangles, and stars with diagonal crosses denote the data measured in the forward rapidity region (in the center-of-mass system) in INEL pp collisions by the NA61/SHINE Collaboration [30] at the SPS, in mid-rapidity interval $|y| < 0.1$ in NSD pp collisions by the STAR Collaboration [3, 31] at the RHIC, in mid-rapidity interval $|y| < 0.5$ in INEL pp collisions by the ALICE Collaboration [32] at the LHC, and in mid-rapidity interval $|y| < 1$ in INEL pp collisions by the CMS Collaboration [33, 34] at the LHC, respec-

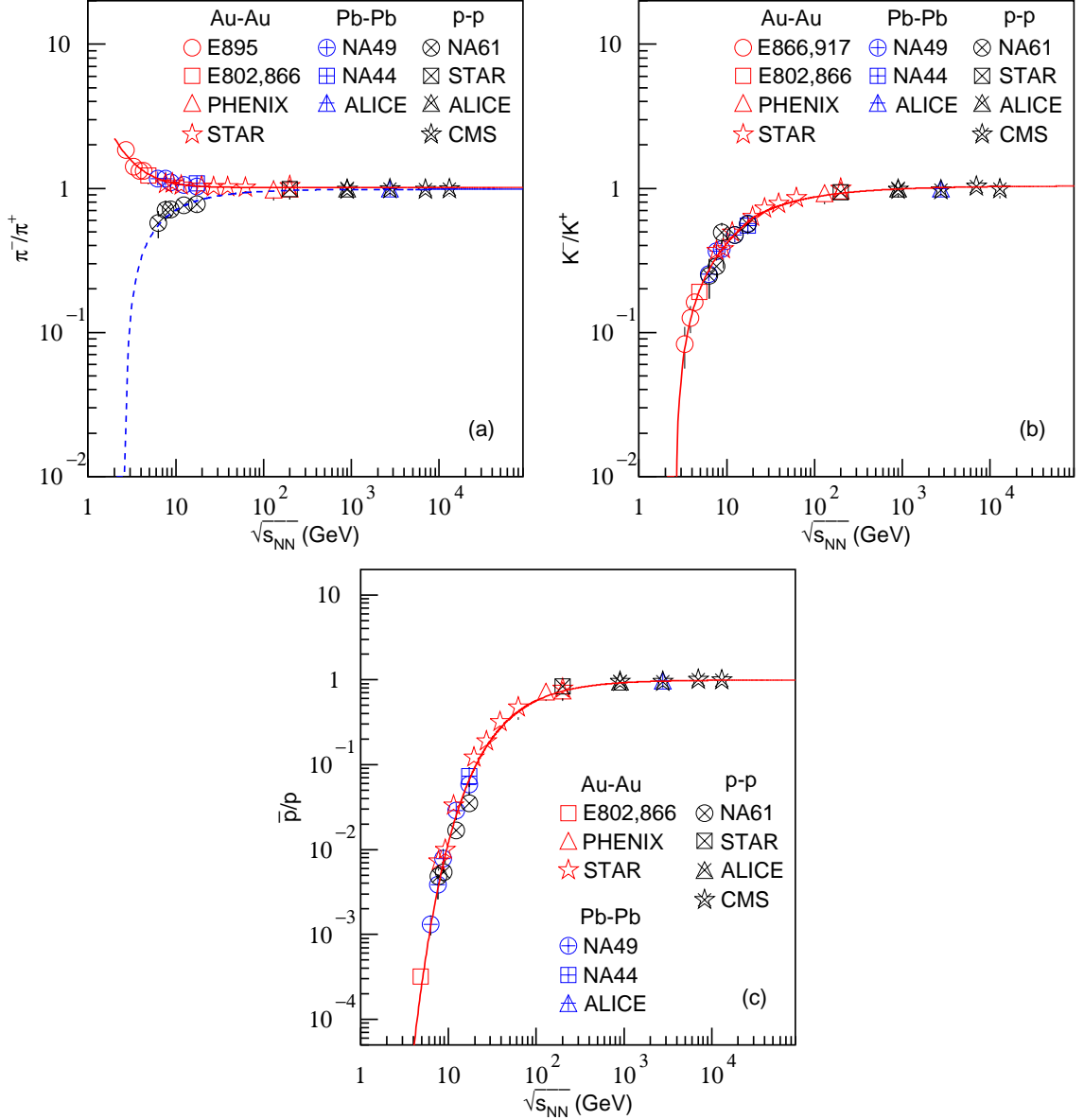


Fig. 1: Yield ratios, (a) π^-/π^+ , (b) K^-/K^+ , and (c) \bar{p}/p , of antiparticles to particles produced in mid-rapidity interval (in most cases) in central Au-Au (Pb-Pb) and INEL or NSD pp collisions at high energies. The symbols denote the data measured in different collisions by different collaborations marked in the panels, where the idiographic references are indexed in the text. In particular, the NA61/SHINE data appear in the forward rapidity region (in the center-of-mass system, though the experiment can provide results with 4π geometry). The solid and dashed curves in Fig. 1(a) are the results fitted by us for the $\sqrt{s_{NN}}$ dependent π^-/π^+ in central Au-Au (Pb-Pb) and INEL or NSD pp collisions respectively. The solid curves in Figs. 1(b) and 1(c) are the results fitted by us for the $\sqrt{s_{NN}}$ dependent K^-/K^+ and \bar{p}/p respectively, for the combining central Au-Au (Pb-Pb) and INEL or NSD pp collisions.

tively. The solid and dashed curves in Fig. 1(a) are the results fitted by us for the $\sqrt{s_{NN}}$ dependent π^-/π^+ in central Au-Au (Pb-Pb) and INEL or NSD pp collisions respectively. The solid curves in Figs. 1(b) and 1(c) are the results fitted by us for the $\sqrt{s_{NN}}$ dependent K^-/K^+

and \bar{p}/p respectively, for the combining central Au-Au (Pb-Pb) and INEL or NSD pp collisions.

It should be noted that the π^-/π^+ ratios presented in Fig. 1(a) obtained by the NA61/SHINE Collaboration from pp collisions at around 10 GeV are so different

to the others obtained from Au-Au (Pb-Pb) collisions at the same energy. This is due to the resonance decay existed mainly in nucleus-nucleus collisions over an energy range from a few GeV to dozens of GeV [42]. There are secondary cascade collisions between produced particles and subsequent nucleons in nucleus-nucleus collisions, which can produce resonances which then decay and affect mainly π^-/π^+ ratios. For K^-/K^+ and \bar{p}/p ratios presented in Figs. 1(b) and 1(c) respectively, the effect of resonance decay in nucleus-nucleus collisions is not obvious. At very high energy (above 100 GeV), the contribution of resonances can be neglected, which renders similar results in pp and Au-Au (Pb-Pb) collisions. In addition, more energies are deposited in Au-Au (Pb-Pb) collisions than in pp collisions, which also results the difference in π^-/π^+ ratios. Meanwhile, the deposited energies are not too large, which does not result in the difference in K^-/K^+ (\bar{p}/p) ratios.

One can see from Fig. 1 that, with the increase of $\sqrt{s_{NN}}$, π^-/π^+ decreases obviously in central Au-Au (Pb-Pb) collisions and it increases obviously in INEL or NSD pp collisions, and K^-/K^+ and \bar{p}/p increase obviously in both central Au-Au (Pb-Pb) and INEL or NSD pp collisions. The limiting values of the three yield ratios is 1 at very high energy. The solid and dashed curves in Fig. 1(a) can be empirically described by

$$\frac{\pi^-}{\pi^+} = (4.212 \pm 0.682) \cdot (\sqrt{s_{NN}})^{-(1.799 \pm 0.152)} + (1.012 \pm 0.019) \quad (7)$$

and

$$\frac{\pi^-}{\pi^+} = -(2.453 \pm 0.292) \cdot (\sqrt{s_{NN}})^{-(0.943 \pm 0.057)} + (0.984 \pm 0.009) \quad (8)$$

respectively, with χ^2/dof (χ^2 per degree of freedom) to be 0.162 and 1.559 respectively. The solid curves in Figs. 1(b) and 1(c) can be empirically described by

$$\begin{aligned} \frac{K^-}{K^+} = & \left[-(0.291 \pm 0.028) + (0.306 \pm 0.010) \cdot \ln(\sqrt{s_{NN}}) \right] \\ & \cdot \theta(20 - \sqrt{s_{NN}}) \\ & + \left[-(2.172 \pm 0.146) \cdot (\sqrt{s_{NN}})^{-(0.554 \pm 0.018)} \right. \\ & \left. + (1.039 \pm 0.016) \right] \\ & \cdot \theta(\sqrt{s_{NN}} - 20) \end{aligned} \quad (9)$$

and

$$\begin{aligned} \frac{\bar{p}}{p} = & \exp \left[-(34.803 \pm 3.685) \cdot (\sqrt{s_{NN}})^{-(0.896 \pm 0.041)} \right. \\ & \left. - (0.008 \pm 0.004) \right] \end{aligned} \quad (10)$$

respectively, with χ^2/dof to be 2.735 and 7.715 respectively. According to these functions, by using Eqs. (5) and (6), the chemical potentials of light particles and quarks can be obtained.

Figures 2(a), 2(b), and 2(c) present respectively the chemical potentials, μ_π , μ_K , and μ_p , of π , K , and p produced in mid-rapidity interval (in most cases) in central Au-Au (Pb-Pb) and INEL or NSD pp collisions at high energies. The symbols denote the derivative data obtained from Fig. 1 according to Eq. (5), where different symbols correspond to different collaborations marked in the panels which are the same as Fig. 1. For the purpose of comparison, the normal, medium, and small symbols with diagonal crosses denote the derivative data in INEL or NSD pp collisions obtained by T_{ch} , $0.9T_{ch}$, and $0.8T_{ch}$ in Eq. (5), respectively, due to the fact that the chemical freeze-out temperature in pp collisions is not available. The curves are the derivative results obtained from the curves in Fig. 1 according to Eq. (5). The solid and dashed curves in Fig. 2(a) are the derivative results for central Au-Au (Pb-Pb) and INEL or NSD pp collisions respectively. The solid curves in Figs. 2(b) and 2(c) are the derivative results for the combining central Au-Au (Pb-Pb) and INEL or NSD pp collisions. One can see that, with the increase of $\sqrt{s_{NN}}$ over a range from above a few GeV to above 10 TeV, μ_π increases obviously in central Au-Au (Pb-Pb) collisions and it decreases obviously in INEL or NSD pp collisions, and μ_K and μ_p decrease obviously in both central Au-Au (Pb-Pb) and INEL or NSD pp collisions. The limiting values of the three types of chemical potentials are 0 at very high energy. As derivative results from Fig. 1, the difference and similarity in pp and Au-Au (Pb-Pb) collisions are natural due to the application of Eq. (5).

Figure 3 is the same as Fig. 2, but Figs. 3(a), 3(b), and 3(c) present respectively the chemical potentials, μ_u , μ_d , and μ_s , of u , d , and s quarks, which are derived from mid-rapidity interval (in most cases) in central Au-Au (Pb-Pb) and INEL or NSD pp collisions at high energies. The symbols denote the derivative data obtained from Fig. 1 according to Eq. (6), where different symbols correspond to different collaborations marked in the panels which are the same as Figs. 1 and 2. For the purpose of comparison, the normal, medium, and small symbols with diagonal crosses denote the derivative data in INEL or NSD pp collisions obtained by T_{ch} , $0.9T_{ch}$, and $0.8T_{ch}$ in Eq. (6), respectively. The curves are the derivative results obtained from the curves in Fig. 1 according to Eq. (6), where the solid and dashed

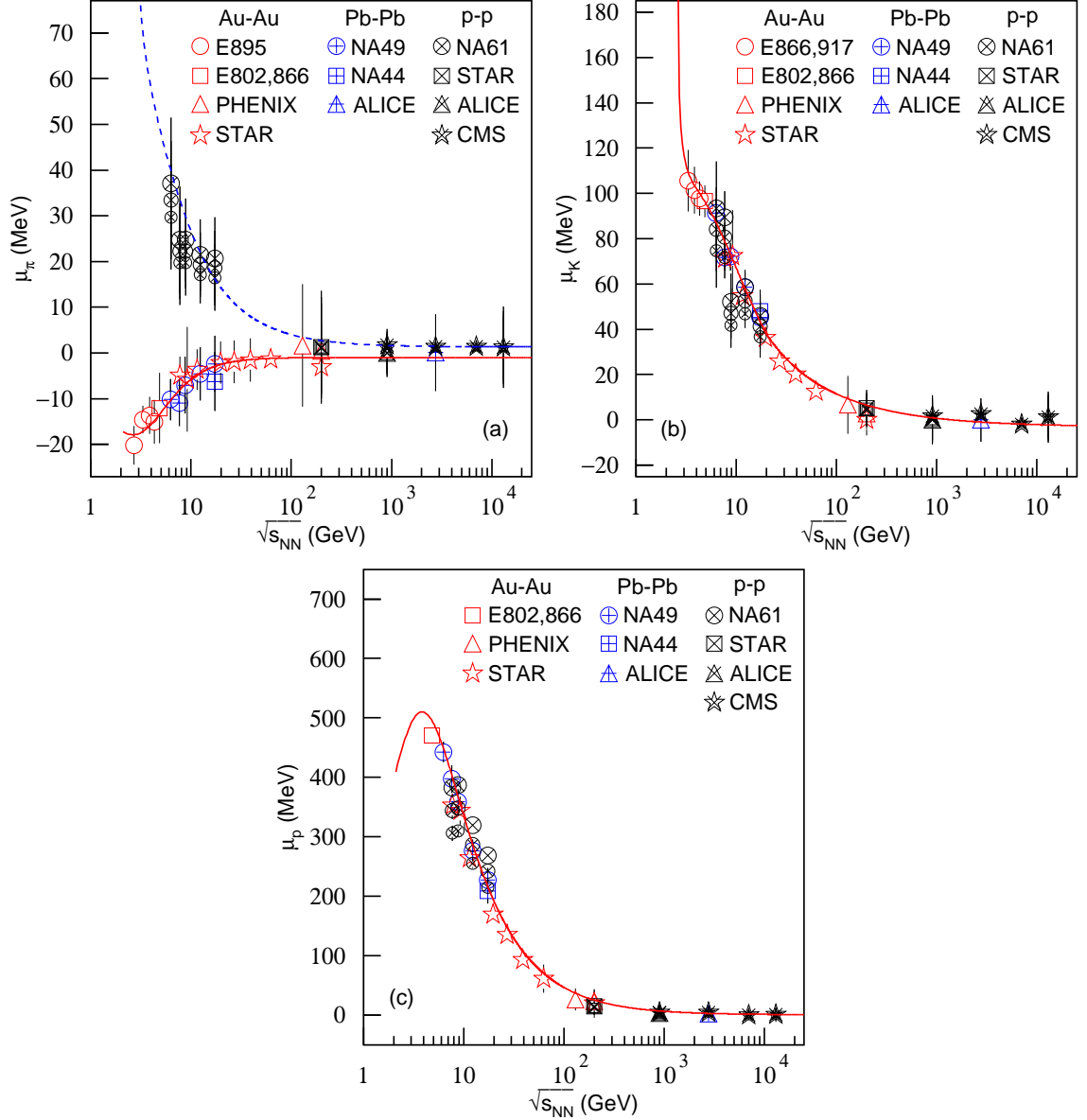


Fig. 2: Chemical potentials, (a) μ_{π} , (b) μ_K , and (c) μ_p , of (a) π , (b) K , and (c) p produced in mid-rapidity interval (in most cases) in central Au-Au (Pb-Pb) and INEL or NSD pp collisions at high energies. The symbols denote the derivative data obtained from Fig. 1 according to Eq. (5). In particular, the NA61/SHINE data appear in the forward rapidity region (in the center-of-mass system), though the experiment can provide results with 4π geometry. The normal, medium, and small symbols with diagonal crosses denote the derivative data in INEL or NSD pp collisions obtained by T_{ch} , $0.9T_{ch}$, and $0.8T_{ch}$ in Eq. (5), respectively. The curves surrounded the symbols are the derivative results obtained from the curves in Fig. 1 according to Eq. (5).

curves are for central Au-Au (Pb-Pb) and INEL or NSD pp collisions respectively. One can see that, with the increase of $\sqrt{s_{NN}}$ over a range from above a few GeV to above 10 TeV, μ_u , μ_d , and μ_s decrease obviously in both central Au-Au (Pb-Pb) and INEL or NSD pp collisions. The limiting values of the three chemical potentials are 0 at very high energy.

In Fig. 2, at a few GeV (~ 4 GeV), some curves show different trends comparing with those at other energies, which are not observed from the curves of the yield ratios in Fig. 1. At the same time, the curves in Fig. 3 also show different trends at a few GeV. Indeed, this energy is a special energy. In our opinion, these special trends appear due to this energy being the ini-

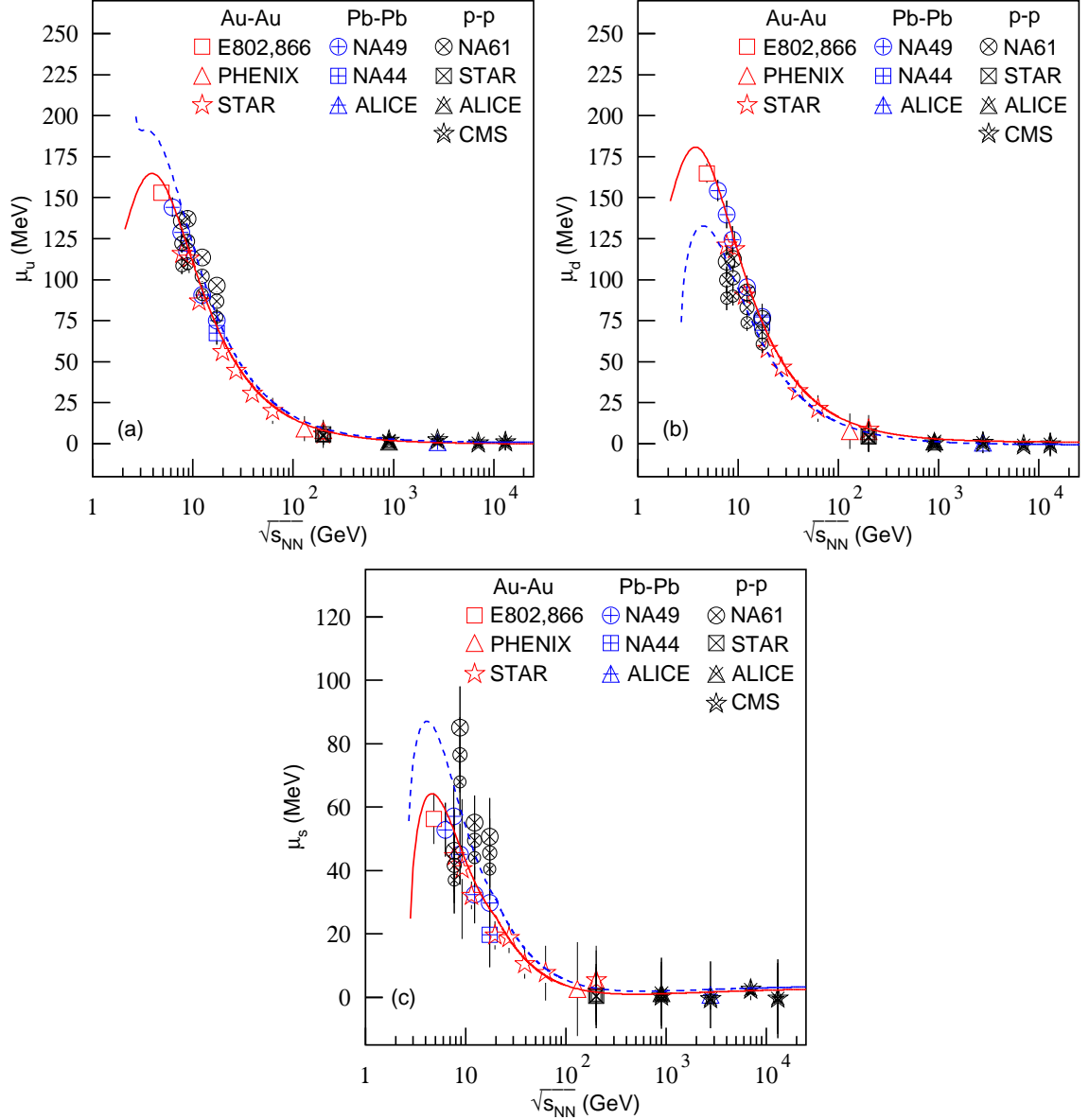


Fig. 3: Chemical potentials, (a) μ_u , (b) μ_d , and (c) μ_s , of (a) u , (b) d , and (c) s quarks derived from mid-rapidity interval (in most cases) in central Au-Au (Pb-Pb) and INEL or NSD pp collisions at high energies. The symbols denote the derivative data obtained from Fig. 1 according to Eq. (6). In particular, the NA61/SHINE data appear in the forward rapidity region (in the center-of-mass system), though the experiment can provide results with 4π geometry. The normal, medium, and small symbols with diagonal crosses denote the derivative data in INEL or NSD pp collisions obtained by T_{ch} , $0.9T_{ch}$, and $0.8T_{ch}$ in Eq. (6), respectively. The curves surrounded the symbols are the derivative results obtained from the curves in Fig. 1 according to Eq. (6).

tial energy of limiting fragmentation of collision nuclei. This energy is also the energy at which the phase transition from a liquid-like state to a gas-like state in the collision system is expected to happen initially, where the liquid-like state is a state in which the mean-free-path of interacting particles is relatively short, and the gas-like state is a state in which the mean-free-path of

interacting particles is relatively long. In addition, the density of baryon number in nucleus-nucleus collisions at this energy has a large value. Because of these particular factors, the collisions at this energy present different features from other energies. The matter formed at this energy changes initially its state from the liquid-like nucleons and mesons to the gas-like nucleons and mesons

in whole stage of collisions.

The above explanation on the initial energy of limiting fragmentation of collision nuclei or the energy of the phase-transition from the liquid-like state to the gas-like state in the collision system is deservedly to discuss. In fact, the present work contains rather standard analysis, performed since many years [43–46] without too much novel results in the field. The conclusion concerning physics presented in the present work is possibly too far-reaching. Instead, the yield ratios discussed in the present work can be also explained within the statistical hadron resonance gas (HRG) model and the ultrarelativistic quantum molecular dynamics (UrQMD) transport model [43–46]. At a few GeV, the collision system stays at the state with the maximum density and minimum radius, which results different trends of chemical potentials.

From above a few GeV to dozens of GeV, the cases of $k_\pi > 1$ and $\mu_\pi < 0$ in central Au-Au (Pb-Pb) collisions are different from other particles and in INEL or NSD pp collisions. These render the resonant production of pions in central Au-Au (Pb-Pb) collisions, which does not contribute too much to other particles or in INEL or NSD pp collisions [42]. At the RHIC and LHC, the trends of k_π and μ_π in central Au-Au (Pb-Pb) collisions are close to other particles or INEL or NSD pp collisions due to the insignificant contribution to pions and other particles. From above a few GeV to above 10 TeV, the yield ratios approach to 1 and the chemical potentials approach to 0. These render that the mean-free-path of produced particles (quarks) becomes large and the viscous effect becomes weakly at the LHC. The interacting system changes completely from the liquid-like state which is hadron-dominant to the gas-like state which is quark-dominant at the early and medium stage in collisions at very high energy, though the final stage is hadron-dominant gas-like state.

Before giving conclusions, we discuss further the extraction method of chemical potentials. Theoretically, chemical potentials always correspond to some conserved charge. For example, in Ref. [39], it is written how a hadron i has a chemical potential. One has $\mu_i = \mu_{baryon}B_i + \mu_S S_i + \mu_I I_i + \mu_C C_i$, where μ with a lower foot mark corresponds to each chemical potential, and B_i , S_i , I_i , and C_i are the particle's baryon number, strangeness, isospin, and charm, respectively. Although not all of them are free parameters since some of them are fixed by the conservation laws and some of them are 0 for a special particle, it is still lesser-known to determine μ_i . In particular, to determine the chemical

potentials of quarks is more lesser-known.

To determine the chemical potentials, the present work tries to use a convenient method. In the case of utilizing T_{ch} , chemical potentials are obtained according to the yield ratios of antiparticles to particles. In the extraction, the difference between the chemical potentials of antiparticles and particles is neglected, and the difference between the chemical potentials of quark and its anti-quark is also neglected. Then, Eqs. (1), (3), and (4) are acceptable. In addition, we have used a single- T_{ch} scenario for the chemical freeze-out, though a two- T_{ch} (or multi- T_{ch}) scenario is also possible. In most cases, one intends to use the single- T_{ch} scenario for the chemical freeze-out.

4 Conclusions

In summary, we have collected the yield ratios, π^-/π^+ , K^-/K^+ , and \bar{p}/p , of antiparticles to particles produced in mid-rapidity interval (in most cases) in central Au-Au (Pb-Pb) and INEL or NSD pp collisions over an energy range from a few GeV to above 10 TeV. It is shown that, with the increase of $\sqrt{s_{NN}}$, π^-/π^+ decreases obviously in central Au-Au (Pb-Pb) collisions and it increases obviously in INEL or NSD pp collisions, and K^-/K^+ and \bar{p}/p increase obviously in both central Au-Au (Pb-Pb) and INEL or NSD pp collisions. The limiting values of the three yield ratios is 1 at very high energy.

The chemical potentials of light particles and quarks are extracted from the yield ratios. With the increase of $\sqrt{s_{NN}}$ over a range from above a few GeV to above 10 TeV, μ_π increases obviously in central Au-Au (Pb-Pb) collisions and it decreases obviously in INEL or NSD pp collisions, and μ_K and μ_p decrease obviously in both central Au-Au (Pb-Pb) and INEL or NSD pp collisions. Meanwhile, μ_u , μ_d , and μ_s decrease obviously in both central Au-Au (Pb-Pb) and INEL or NSD pp collisions. The limiting values of the chemical potentials of the three types of light particles and the three flavors of light quarks are 0 at very high energy.

At a few GeV (~ 4 GeV), some curves of the chemical potentials show different trends which are not observed from the curves of the yield ratios. These special trends appear due to this energy being possibly the initial energy of limiting fragmentation of collision nuclei. This energy is also the energy of the phase transition from the liquid-like state to the gas-like state in the collision system. The interacting system changes com-

pletely from the hadron-dominant liquid-like state to the quark-dominant gas-like state at the early and medium stage in collisions at very high energy.

The yield ratios discussed in the present work can also be explained within the statistical hadron resonance gas model and the ultrarelativistic quantum molecular dynamics transport model [43–46]. At a few GeV, the collision system stays at the state with the maximum density and minimum radius, which results different trends of chemical potentials. The density of baryon number in nucleus-nucleus collisions at a few GeV has a large value. These particular factors render different features at this energy.

Data Availability

The data used to support the findings of this study are quoted from the mentioned references. As a phenomenological work, this paper does not report new data.

Conflicts of Interest

The authors declare that there are no conflicts of interest regarding the publication of this paper.

Acknowledgments

This work was supported by the National Natural Science Foundation of China under Grant Nos. 11575103, 11747319, and 11847311, the Scientific and Technological Innovation Programs of Higher Education Institutions in Shanxi (STIP) under Grant No. 201802017, the Shanxi Provincial Natural Science Foundation under Grant No. 201701D121005, the Fund for Shanxi “1331 Project” Key Subjects Construction, and the Doctoral Scientific Research Foundation of Taiyuan University of Science and Technology under Grant No. 20152043.

References

- [1] Cleymans, J.; Oeschler, H.; Redlich, K.; Wheaton, S. Comparison of chemical freeze-out criteria in heavy-ion collisions. *Phys. Rev. C* **2006**, *73*, 034905.
- [2] Andronic, A.; Braun-Munzinger, P.; Stachel, J. The horn, the hadron mass spectrum and the QCD phase diagram: the statistical model of hadron production in central nucleus-nucleus collisions. *Nucl. Phys. A* **2010**, *834*, 237c–240c.
- [3] Adameczyk, L.; et al. [STAR Collaboration] Bulk properties of the medium produced in relativistic heavy-ion collisions from the beam energy scan program. *Phys. Rev. C* **2017**, *96*, 044904.
- [4] Bellwied, R. Sequential strangeness freeze-out. *EPJ Web Conf.* **2018**, *171*, 02006.
- [5] Turko, L. [for the NA61/SHINE Collaboration] Looking for the phase transition — recent NA61/SHINE results. *Universe* **2018**, *4*, 52.
- [6] Grebieszko, K. [for the NA61/SHINE Collaboration] News from strong interactions program of the NA61/SHINE experiment. *Acta Phys. Pol. B Proc. Suppl.* **2017**, *10*, 589–596.
- [7] Xu, N. [for the STAR Collaboration] An overview of STAR experimental results. *Nucl. Phys. A* **2014**, *931*, 1–12.
- [8] Yang, C. [for the STAR Collaboration] The STAR beam energy scan phase II physics and upgrades. *Nucl. Phys. A* **2017**, *967*, 800–803.
- [9] Arslanovic, M. [for the ALICE Collaboration] Event-by-event identified particle ratio fluctuations in Pb-Pb collisions with ALICE using the identity method. *Nucl. Phys. A* **2017**, *956*, 870–873.
- [10] Aaij, R.; et al. [LHCb collaboration] Measurement of the inelastic pp cross-section at a centre-of-mass energy of $\sqrt{s} = 7$ TeV. *J. High Energy Phys.* **2015**, *02*, 129.
- [11] Sirunyan, A.M.; et al. [CMS collaboration] Measurements of differential cross sections of top quark pair production as a function of kinematic event variables in proton-proton collisions at $\sqrt{s} = 13$ TeV. *J. High Energy Phys.* **2018**, *06*, 002.
- [12] Aaboud, M.; et al. [ATLAS Collaboration] Measurements of top-quark pair differential cross-sections in the $e\mu$ channel in pp collisions at $\sqrt{s} = 13$ TeV using the ATLAS detector. *Eur. Phys. J. C* **2017**, *77*, 292.
- [13] Klay, J.L.; et al. [E895 Collaboration] Charged pion production in 2 to 8A GeV central Au+Au collisions *Phys. Rev. C* **2003**, *68*, 054905.
- [14] Ahle, L.; et al. [E866/E917 Collaboration] An excitation function of K^- and K^+ production in Au+Au reactions at the AGS. *Phys. Lett. B* **2000**, *409*, 53–60.
- [15] Klay, J.L.; et al. [E895 Collaboration] Longitudinal flow from (2-8)A GeV Au+Au collisions, *Phys. Rev. Lett.* **2002**, *88*, 102301.
- [16] Akiba, Y. [for the E802 Collaboration] Particle production in Au+Au collisions from BNL E866. *Nucl. Phys. A* **1996**, *610*, 139c–152c.
- [17] Ahle, L.; et al. [E802 Collaboration] Particle production at high baryon density in central Au+Au reactions at 11.6A GeV/c. *Phys. Rev. C* **1998**, *57*, 466–477(R).
- [18] Adcox, K.; et al. [PHENIX Collaboration] Single identified hadron spectra from $\sqrt{s_{NN}}=130$ GeV Au+Au collisions. *Phys. Rev. C* **2004**, *69*, 024904.
- [19] Adcox, K.; et al. [PHENIX Collaboration] Centrality dependence of π^+/π^- , K^+/K^- , p and \bar{p} production

- from $\sqrt{s_{NN}}=13$ GeV Au+Au collisions at RHIC. *Phys. Rev. Lett.* **2002**, 88, 242301.
- [20] Adler S.S.; et al. [PHENIX Collaboration] Identified charged particle spectra and yields in Au+Au collisions at $\sqrt{s_{NN}}=200$ GeV. *Phys. Rev. C* **2004**, 69, 034909.
- [21] Abelev, B.; et al. [STAR Collaboration] Identified particle production, azimuthal anisotropy, and interferometry measurements in Au+Au collisions at $\sqrt{s_{NN}}=9.2$ GeV. *Phys. Rev. C* **2010**, 81, 024911.
- [22] Abelev, B.; et al. [STAR Collaboration] Systematic measurements of identified particle spectra in pp , d +Au and Au+Au collisions from STAR. *Phys. Rev. C* **2009**, 79, 034909.
- [23] Adams, J.; et al. [STAR Collaboration] Identified particle distributions in pp and Au+Au collisions at $\sqrt{s_{NN}}=200$ GeV. *Phys. Rev. Lett.* **2004**, 92, 112301.
- [24] Alt, C.; et al. [NA49 Collaboration] Pion and kaon production in central Pb+Pb collisions at 20A and 30A GeV: evidence for the onset of deconfinement. *Phys. Rev. C* **2008**, 77, 024903.
- [25] Afanasiev, S.V.; et al. [NA49 Collaboration] Energy dependence of pion and kaon production in central Pb+Pb collisions. *Phys. Rev. C* **2002**, 66, 054902.
- [26] Alt, C.; et al. [NA49 Collaboration] Energy and centrality dependence of \bar{p} and p production and the \bar{L}/\bar{p} ratio in Pb+Pb collisions between 20A GeV and 158A GeV. *Phys. Rev. C* **2006**, 73, 044910.
- [27] Afanasiev, S.V.; et al. [NA49 Collaboration] Energy and centrality dependence of deuteron and proton production in Pb+Pb collisions at relativistic energies. *Phys. Rev. C* **2004**, 69, 024902.
- [28] Bearden, I.G.; et al. [NA44 Collaboration] Particle production in central Pb+Pb collisions at 158A GeV/c. *Phys. Rev. C* **2002**, 66, 044907.
- [29] Abelev, B.; et al. [ALICE Collaboration] Centrality dependence of π , K , p production in Pb-Pb collisions at $\sqrt{s_{NN}}=2.76$ TeV. *Phys. Rev. C* **2013**, 88, 044910.
- [30] Aduszkiewicz, A.; et al. [NA61/SHINE Collaboration] Measurements of π^\pm , K^\pm , p and \bar{p} spectra in proton-proton interactions at 20, 31, 40, 80 and 158 GeV/c with the NA61/SHINE spectrometer at the CERN SPS. *Eur. Phys. J. C* **2017**, 77, 671.
- [31] Abelev, B.I.; et al. [STAR Collaboration] Strange particle production in $p+p$ collisions at $\sqrt{s}=200$ GeV. *Phys. Rev. C* **2007**, 75, 064901.
- [32] Aamodt, K.; et al. [ALICE Collaboration] Production of pions, kaons and protons in pp collisions at $\sqrt{s}=900$ GeV with ALICE at the LHC. *Eur. Phys. J. C* **2011**, 71, 1655.
- [33] Chatrchyan, S.; et al. [CMS Collaboration] Study of the inclusive production of charged pions, kaons, and protons in pp collisions at $\sqrt{s}=0.9, 2.76, \text{ and } 7$ TeV. *Eur. Phys. J. C* **2012**, 72, 2164.
- [34] Sirunyan, A.M.; et al. [CMS Collaboration] Measurement of charged pion, kaon, and proton production in proton-proton collisions at $\sqrt{s}=13$ TeV. *Phys. Rev. D* **2017**, 96, 112003.
- [35] Gao, Y.-Q.; Lao, H.-L.; Liu, F.-H. Chemical potentials of light flavor quarks from yield ratios of negative to positive particles in Au+Au collisions at RHIC. *Adv. High Energy Phys.* **2018**, 2018, 6047960.
- [36] Koch, P.; Rafelski, J.; Greiner, W. Strange hadron in hot nuclear matter. *Phys. Lett. B* **1983**, 123, 151–154.
- [37] Braun-Munzinger, P.; Magestro, D.; Redlich, K.; Stachel, J. Hadron production in Au-Au collisions at RHIC. *Phys. Lett. B* **2001**, 518, 41–46.
- [38] Andronic, A.; Braun-Munzinger, P.; Stachel, J. Thermal hadron production in relativistic nuclear collisions. *Acta Phys. Pol. B* **2009**, 40, 1005-1012.
- [39] Andronic, A.; Braun-Munzinger, P.; Stachel, J. Hadron production in central nucleus-nucleus collisions at chemical freeze-out. *Nucl. Phys. A* **2006**, 772, 167–199.
- [40] Arsene, I.; et al. [BRAHMS Collaboration] Quark gluon plasma and color glass condensate at RHIC? the perspective from the BRAHMS experiment. *Nucl. Phys. A* **2005**, 757, 1–27.
- [41] Zhao, H.; Liu, F.-H. On extraction of chemical potentials of quarks from particle transverse momentum spectra in high energy collisions. *Adv. High Energy Phys.* **2015**, 2015, 137058.
- [42] Yu, N.; Luo, X.-F. Particle decay from statistical thermal model in high-energy nucleus-nucleus collisions. *Eur. Phys. J. A* **2019**, 55, 26.
- [43] Begun, V.V.; Vovchenko, V.; Gorenstein, M.I.; Stoecker, H.; Motornenko, A. Hadron yields and fluctuations at energies available at the CERN Super Proton Synchrotron: System-size dependence from Pb+Pb to $p+p$ collisions. *Phys. Rev. C* **2019**, 99, 034909.
- [44] Begun, V.V.; Vovchenko, V.; Gorenstein, M.I.; Stoecker, H. Statistical hadron-gas treatment of systems created in proton-proton interactions at energies available at the CERN Super Proton Synchrotron. *Phys. Rev. C* **2018**, 98, 054909.
- [45] Begun, V.V.; Vovchenko, V.; Gorenstein, M.I. Surprises for the chemical freeze-out lines from the new data in $p+p$ and $A+A$ collisions. *Acta Phys. Pol. B Proc. Supp.* **2017**, 10, 467–471.
- [46] Vovchenko, V.; Begun, V.V.; Gorenstein, M.I. Hadron multiplicities and chemical freeze-out conditions in proton-proton and nucleus-nucleus collisions. *Phys. Rev. C* **2016**, 93, 064906.